International Journal of Maritime and Interdisciplinary Research
©2026 IJMIR/Volume 8(3) July - December | ISSN: 2734-3286.

Journal homepage: www.ijmir.edu.ng

ANALYTICAL MODELING AND PARAMETRIC CONTROL OF UNSTEADY MHD ELECTRO-OSMOTIC FLOW OF HYBRID JEFFREY NANOFLUIDS IN POROUS MICROCHANNELS

By

OROVWUJE Paul Stephen[1], ADUMA Onisobuana Cyril[2], AWOYEMI, Sunday Aremu[3], OFILI Augustine Chiedu[4]

Department of Mathematics, Science, Nigeria Maritime University[1,3]

Department of Petroleum and Gas Engineering, Engineering, Nigeria Maritime University[2]

Department of Mathematics, Physical Science, University of Calabar[4]

Corresponding Author: orowwuje.paul@nmu.edu.ng

ABSTRACT

This study develops an analytical model for unsteady magnetohydrodynamic (MHD) electro-osmotic flow of a hybrid Jeffrey nanofluid in a porous microchannel, integrating viscous dissipation, Joule heating, thermal radiation, nonlinear heat generation/absorption, and slip/jump boundary conditions. The governing equations are non-dimensionalized and solved using the semi-analytical He–Laplace method. Parametric analysis reveals that electro-osmotic actuation effectively counteracts magnetic damping (Ha), providing precise flow control. The hybrid nanofluid $(Cu-Al_2O_3/water)$ *demonstrates superior thermal performance, with a* 37.5% *reduction in maximum temperature compared to the base fluid. Key parameters such as the Jeffrey parameter* (λ_1)*, suction or injection* (S)*, Eckert number* (Ec)*, and radiation parameter* (Rd) *significantly influence flow and thermal behavior. The model offers a predictive framework for designing optimized microfluidic cooling systems.*

Keywords: Magnetohydrodynamic, Electro-osmosis, Hybrid nanofluid, Jeffrey fluid, Microchannel, He-Laplace method.

1.0 Introduction

As modern electronic and biomedical devices continue to shrink while delivering more power, controlling the heat they produce is now a critical concern. Microchannel cooling systems, enhanced by sophisticated working fluids and active flow control mechanisms, have emerged as pivotal technologies in this domain. Recent studies demonstrate that hybrid nanofluids [1],

magnetic fields [11], and electro-osmotic actuation [4] can significantly improve thermal efficiency and stability in modern thermal systems.

By combining different types of nanoparticles, hybrid nanofluids provide tunable and often improved thermophysical properties compared to mono-nanofluids [1]. To accurately capture their rheological behavior, which often exhibits both viscous and elastic characteristics, the Jeffrey fluid model is employed [3]. This model incorporates the relaxation and retardation times (λ_1, λ_2) and effectively captures the behavior of polymers, biological media, and other structured fluids.

Magnetohydrodynamic (MHD) effects introduce Lorentz forces that can suppress flow, while electro-osmotic (EO) actuation provides contactless pumping via the electric double layer (EDL) [4]. Combining these with porous-wall effects (suction/injection) and comprehensive heat transfer mechanisms (radiation, viscous dissipation, Joule heating) creates a multiphysical system of high practical relevance.

Previous studies have examined subsets of these phenomena: MHD nanofluid flow [5], EO pumping [6], and hybrid nanofluid heat transfer [7]. However, a unified analytical model combining unsteady MHD-EO flow of a hybrid Jeffrey nanofluid in a porous channel with full thermal coupling remains absent. This work bridges that gap by developing a comprehensive model and obtaining semi-analytical solutions using the He-Laplace method [8, 9]. The results will provide insights into parametric control strategies for advanced micro cooling applications.

2. Mathematical Formulation

2.1 Geometry and Assumptions

Consider an unsteady, incompressible flow between two parallel plates located at $y = \pm H$, driven by a constant pressure gradient $-\frac{\partial p}{\partial x}$, a transverse magnetic field $B_0\,\hat{y}$, and an imposed axial electric field $E_0\,\hat{x}$. The channel walls are porous and allow uniform suction or injection with velocity v_w. The working fluid is a $Cu - Al_2O_3$ hybrid nanofluid, modeled with a total nanoparticle volume fraction $\varphi = \varphi_1 + \varphi_2$, following established hybrid nanofluid formulations and magnetohydrodynamic principles [1, 11, 4].

Remark 1. The following assumptions are adopted:

1. Unidirectional flow: $v = (u(y,t), 0, 0)$
2. Low magnetic Reynolds number (induced magnetic field neglected)
3. Thin EDL (Debye-Huckel approximation valid)
4. Thermal equilibrium between nanoparticles and base fluid
5. Jeffrey fluid rheology with relaxation (λ_1) and retardation (λ_2) times

2.2 Constitutive Equations

Definition 2 (Jeffrey Fluid Model). The extra stress tensor for a Jeffrey fluid satisfies the constitutive equation:

$$\tau + \lambda_1 \frac{\partial \tau}{\partial t} = \mu_{nf} \left(\dot{\gamma} + \lambda_2 \frac{\partial \dot{\gamma}}{\partial t} \right) \quad 2.1$$

where μ_{nf} is the effective dynamic viscosity and $\dot{\gamma}$ is the rate-of-deformation tensor.

For unidirectional flow $v = (u(y,t), 0, 0)$, equation (2.1) reduces to:

$$\tau_{xy} + \lambda_1 \frac{\partial \tau_{xy}}{\partial t} = \mu_{nf} \left(\frac{\partial u}{\partial y} + \lambda_2 \frac{\partial}{\partial t} \left(\frac{\partial u}{\partial y} \right) \right) \quad 2.2$$

2.3 Hybrid Nanofluid Properties

Definition 3 ($Effective\ Properties$). For a hybrid nanofluid containing nanoparticles of types 1 and 2:

$$\rho_{nf} = (1 - \varphi)\rho_f + \varphi_1 \rho_{p1} + \varphi_2 \rho_{p2} \quad 2.3$$

$$(\rho c_p)_{nf} = (1 - \varphi)(\rho c_p)_f + \varphi_1 (\rho c_p)_{p1} + \varphi_2 (\rho c_p)_{p2} \quad 2.4$$

The Brinkman and Maxwell models give:

$$\mu_{nf} = \mu_f (1 - \varphi)^{-2.5} \quad 2.5$$

$$k_{nf} = k_f * \frac{[k_{pe} + 2k_f + 2\varphi(k_{pe} - k_f)]}{[k_{pe} + 2k_f - \varphi(k_{pe} - k_f)]} \quad 2.6$$

Where $k_{pe} = (\varphi_1 k_{p1} + \varphi_2 k_{p2})/\varphi$.

2.4 Governing Equations (Dimensional Form)

Theorem 4 (Momentum Equation). The momentum equation for unsteady Jeffrey hybrid nanofluid flow is:

$$\rho_{nf} \frac{\partial u}{\partial t} = -\frac{\partial p}{\partial x} + \frac{\partial \tau_{xy}}{\partial y} - \left(\frac{\mu_{nf}}{K} \right) u - \sigma_e B_0^2 u + \rho_e E_0 \quad 2.7$$

where $\rho_e = -\varepsilon \kappa^2 \psi$ from the Poisson-Boltzmann equation [11, 4, 5].

Theorem 5 (Energy Equation). The energy equation including comprehensive thermal effects is:

$$(\rho c_p)_{nf} \frac{\partial T}{\partial t} = k_{nf} \frac{\partial^2 T}{\partial y^2} + \tau_{xy} \frac{\partial u}{\partial y} + \sigma_e E^{02} + \frac{16\sigma^* T_\infty^3}{(3k^*)} \frac{\partial^2 T}{\partial y^2} + Q_0 (T - T_\infty) \quad 2.8$$

(The effective thermophysical properties correspond to a $Cu - Al_2O_3$ hybrid nanofluid. The inclusion of Joule heating, viscous dissipation, and Rosseland thermal radiation is consistent with established thermal transport models in MHD and nanofluid literature [1, 3, 5].)

2.5 Boundary and Initial Conditions

Condition 6 (Boundary Conditions). Slip and temperature jump at walls:

$$u \pm l_s \frac{\partial u}{\partial y} = \pm v_w + u_{eo}, \qquad y = \pm H \tag{2.9}$$

$$T \pm l_T \frac{\partial T}{\partial y} = T_w, \qquad y = \pm H \tag{2.10}$$

$with\ u_{eo} = -\varepsilon E_0 \zeta / \mu_nf$.

Condition 7 (Initial Conditions).

$$u(y,0) = 0 \tag{2.11}$$

$$T(y,0) = T_\infty \tag{2.12}$$

2.6 Non-Dimensionalization

Introduce dimensionless variables [11, 6]:

$$Y = \frac{y}{H},\ U = \frac{u}{\cup_0},\ \tau = \frac{\nu_f t}{H^2},\ \Theta = \frac{T - T_\infty}{(T_w - T_\infty)},\ \Psi = \frac{\psi}{\zeta}$$

Definition 8 (Dimensionless Groups). Key dimensionless parameters:

$$Re = \frac{\rho_f U_0 H}{\mu_f},\quad Ha = B_0 H \sqrt{\frac{\sigma_e}{\mu_f}},\quad m = \kappa H,\ Da = \frac{K}{H^2},\ \Lambda_{1,2} = \frac{\lambda_{1,2}\nu_f}{H^2},\quad S = \frac{v_w H}{v_f}$$

$$Pr = \frac{\mu_f c_{p,f}}{k_f},\ Ec = \frac{\cup_0^2}{c_{p,f}\Delta T},\ Rd = \frac{16\sigma^* T_\infty^3}{(3k^* k_f)},\ J = \frac{\sigma_e E^{02} H^2}{(k_f \Delta T)},\ \beta_{s,t} = \frac{l_{s,T}}{H}$$

2.7 Dimensionless Equations

Theorem 9 (Dimensionless Momentum Equation).with the above definitions, the momentum becomes;

$$R\frac{\partial U}{\partial \tau} = G + \frac{\partial}{\partial Y}\left[\mu_r \left(\frac{\partial U}{\partial Y} + \Lambda_2 \frac{\partial^2 U}{\partial \tau \partial Y}\right)\right] - \Lambda_1 \frac{\partial}{\partial \tau}\left[\mu_r \left(\frac{\partial U}{\partial Y} + \Lambda_2 \frac{\partial^2 U}{\partial \tau \partial Y}\right)\right] - \left(\frac{\mu_r}{Da}\right) U$$
$$- Ha^2 U + m^2 \Psi \tag{2.13}$$

$where\ R = \left(\frac{\rho_{nf}}{\rho_f}\right) Re,\quad \mu_r = \frac{\mu_{nf}}{\mu_f},\ and\ \Psi = \frac{cosh(mY)}{cosh(m)}.$

Theorem 10 (Dimensionless Energy Equation). The energy equation is:

$$(\rho c_p)_r \frac{\partial \Theta}{\partial \tau} = \left(\frac{1}{Pr}\right)\left(k_r + \frac{Rd}{1+Rd}\right)\frac{\partial^2 \Theta}{\partial Y^2} + Ec\,\mu_r \left(\frac{\partial U}{\partial Y}\right)^2 + J + Q\,\Theta \tag{2.14}$$

$with\ (\rho c_p)_r = \frac{(\rho c_p)_{nf}}{(\rho c_p)_f},\ and\ k_r = \frac{k_{nf}}{k_f}$

The inclusion of viscous dissipation, Joule heating, and nonlinear thermal radiation follows standard thermal transport models in nanofluid and MHD flow analyses [3; 5; 1]

3. Solution Methodology: He-Laplace Technique

The coupled nonlinear partial differential equations (2.13) and (2.14) are solved analytically using the He-Laplace method, which combines the Laplace transform with the homotopy perturbation framework to efficiently handle temporal derivatives and nonlinear effects [8, 9]. This hybrid approach offers distinct advantages over conventional perturbation techniques, as it does not require the presence of a small parameter in the governing equations, making it particularly suitable for problems involving strong nonlinearities arising from viscous dissipation and Joule heating.

3.1 Laplace Transform

To initiate the analytical procedure, we apply the Laplace transform with respect to the temporal variable τ, defined as :

$$L\{f(\tau)\} = \underline{\bar{f}}(s) = \int_0^{\infty} e^{-s\tau} f(\tau) d\tau \qquad 3.1$$

Lemma 11 (Transformed Equations). Under this transformation, the momentum and energy equations reduce to the following system of ordinary differential equations in the spatial coordinate Y:

Momentum Equation

$$Rs\underline{U} = \frac{G}{s} + \mu_r (1 + \Lambda^2 s)\bar{U}_{YY} - \Lambda_1 s\,[\mu_r(1 + \Lambda^2 s)\bar{U}_{YY}]$$

$$- \left(\frac{\mu_r}{Da}\right)\underline{\bar{U}} - Ha^2\underline{\bar{U}} + \left(\frac{m^2}{s}\right)\Psi(Y) \qquad 3.2$$

Energy Equation

$$(\rho c_p)_r s\bar{\theta} = \left(\frac{1}{Pr}\right)(k_r(1 + Rd))\bar{\theta}_{YY} + Ec\,\mu_r L\left\{\left(\frac{\partial U}{\partial Y}\right)^2\right\} + \frac{I}{s} + Q\,\bar{\theta} \qquad 3.3$$

The transformed equations reveal several important features of the system. The terms involving λ_1 *and* λ_2 capture the viscoelastic characteristics of the Jeffrey fluid, while the combination of $\mu r/Da$ *and* Ha^2 represents the combined resistive effects of the porous medium and the magnetic field, respectively. The electro-osmotic body force is manifested through the term $\left(\frac{m^2}{s}\right)\Psi(Y)$, which couples the flow dynamics to the electric double layer structure.

3.2 Homotopy Perturbation

To obtain analytical solutions of the coupled nonlinear system, the He–Laplace technique is employed. This method combines the Laplace transform with the homotopy perturbation framework, enabling the systematic treatment of nonlinearities without linearization or small-parameter assumptions. The fundamental idea behind the homotopy perturbation method is to

construct a homotopy that continuously deforms a simple problem with known solution into the original complex problem.

Algorithm 12 (He-Laplace Procedure). We introduce the homotopy parameter $p \in [0,1]$ and expand the transformed fields as power series:

$$\underline{U} = \sum_{n=0}^{\infty} \quad p^n \underline{\cup}_n, \qquad \underline{\Theta} = \sum_{n=0}^{\infty} \quad p^n \underline{\Theta}_n \tag{3.4}$$

The nonlinear viscous dissipation term is decomposed using He's polynomials:

$$L'\left\{\left(\frac{\partial U}{\partial Y}\right)^2\right\} = \sum_{n=0}^{\infty} \quad p^n H_n(\underline{\cup}_0, \underline{\cup}_1, \underline{\cup}_2, \cdots) \tag{3.5}$$

The first few He polynomials are:

$$H_0 = L\left\{\left(\underline{\cup}_{0Y}\right)^2\right\}, \qquad H_1 = L\{2\,\underline{\cup}_{0Y}\underline{\cup}_{1Y}\}, \ldots \tag{3.6}$$

These polynomials are systematically constructed to group all terms of the same order in p, ensuring that the nonlinearity is distributed across successive approximations rather than being treated in a single step. This decomposition is particularly advantageous for the viscous dissipation term, which couples the velocity field to the energy equation.

Substitution of the series representations into the Laplace-transformed equations (3.2)-(3.3) and comparison of coefficients of like powers of pp lead to a sequence of linear ordinary differential equations. These equations are solved recursively to obtain successive approximations. The zeroth-order problems capture the dominant physics, while higher-order corrections refine the solution progressively.

The zeroth order problems are as follow:

1. **Momentum (zeroth order):**

$$Rs\underline{U} = \frac{G}{s} + \mu_r\,(1 + \Lambda^2 s)\bar{U}_{0YY} - \Lambda_1 s\,[\mu_r(1 + \Lambda^2 s)\bar{U}_{YY}]$$
$$- \left(\frac{\mu_r}{Da}\right)\underline{\bar{U}}_0 - Ha^2\underline{\bar{U}}_0 + \left(\frac{m^2}{s}\right)\Psi(Y) \tag{3.7}$$

2. **Energy (zeroth order):**

$$(\rho c_p)_r s\bar{\theta}_0 = \left(\frac{1}{Pr}\right)(k_r(1 + Rd))\bar{\theta}_{0YY} + \frac{J}{s} + Q\bar{\theta}_0 \tag{3.8}$$

It is noteworthy that the zeroth-order energy equation already incorporates the Joule heating term $\frac{J}{s}$, which represents the heat generated by the electric current passing through the fluid. However, the viscous dissipation term, being quadratic in the velocity, only appears at higher orders.

3. **Momentum (first order):**

$$Rs\underline{U}_1 = \mu_r(1+\Lambda_2 s)\bar{U}_{1YY} - \Lambda_1 s\,[\mu_r(1+\Lambda_2 s)\bar{U}_{1YY}] - \left(\frac{\mu_r}{Da}\right)\underline{\bar{U}}_1 - Ha^2\underline{\bar{U}}_1 \qquad 3.9$$

4. **Energy (first order):**

$$(\rho c_p)_r s\bar{\theta}_1 = \left(\frac{1}{Pr}\right)(k_r(1+Rd))\bar{\theta}_{1YY} + Ec\,\mu_r H_0 + Q\bar{\theta}_1 \qquad 3.10$$

The boundary conditions for the zeroth-order system are the full inhomogeneous ones (2.9)–(2.10), while higher-order systems satisfy homogeneous versions of these boundary conditions, ensuring that the cumulative solution consistently satisfies the physical constraints imposed at the boundaries.

Explicit Solution $\underline{\cup}_0(Y,s)$

$$\Phi(s) = Rs + \frac{\mu_r}{Da} + Ha^2, \qquad q = \sqrt{\frac{\Phi(s)}{\mu_r(1+\Lambda_2 s)(1-\Lambda_1 s)}}, \quad k = \frac{m^2}{s\Phi(s)} \qquad 3.11$$

Then the particular solution from the EO term is $\frac{Kcosh(mY)}{cosh(m)}$ the pressure term contributes $\frac{G}{s\Phi(s)}$,

Thus:

$$\underline{\cup}_0(Y,s) = C(s)cosh(qY) + \frac{G}{s\Phi(s)} + K\frac{cosh(mY)}{cosh(m)} \qquad 3.12$$

where $C(s)$ is determined from the slip boundary condition (2.9) in Laplace domain:

$$\underline{\cup}_0 \pm \beta_s \frac{\partial\,\underline{\cup}_0}{\partial Y} = \pm\frac{S}{s} + \frac{1}{s} \quad at\ Y = \pm 1 \qquad 3.13$$

Using symmetry (U_0 *even in* Y), we obtain:

$$C(s) = \frac{\frac{S}{s}+\frac{1}{s}\frac{G}{s\Phi(s)} - Kcosh(mY) - \beta_s Kmsinh(m)}{coshcosh\,(q) + \beta_s qsinh(q)} \qquad 3.14$$

Explicit solution for $\bar{\theta}_0(Y,s)$

Define $\gamma = \sqrt{\frac{P_r(\rho c_p)_r s - Q}{K_r(1+Rd)}}$. The particular solution from the joule term is $\frac{J}{[s((}\rho c_p)_\tau s - Q)]$.

Hence:

$$\bar{\theta}_0(Y,s) = D(s)\,cosh\,cosh\,(\gamma Y) + \frac{J}{[s((\rho c_p)_\tau}s - Q)\,] \qquad 3.15$$

where $D(s)$ follows from the temperature jump condition (2.10) in Laplace domain:

$$\bar{\theta}_0 \pm \beta_t \frac{\partial\bar{\theta}_0}{\partial Y} = \frac{1}{s} \quad at\ Y = \pm 1 \qquad 3.16$$

Using symmetry ($\bar{\theta}_0$ even)

$$D(s) = \frac{\frac{1}{s} \quad \frac{I}{s((\rho c_p)_f s - Q}}{coshcosh\,(\gamma Y) + \beta_t \gamma sinh(\gamma)} \qquad 3.17$$

Since the momentum equation is linear, $\underline{\cup}_1 \equiv 0$ for this problem (all source terms are already accounted for in the zeroth-order solution). Thus the velocity series terminates at $n = 0$:

$$\cup (Y, \tau) = U_0(Y, \tau)$$

For temperature, the first-order correction comes from viscous dissipation:

$$\bar{\theta}_1(Y, s) = E(s)\, cosh\, cosh\,(\gamma Y) + Particular\ solution\ of\ 3.8$$

The particular solution is found by expressing $H0$ in terms of $cosh\, cosh\,(2qY)$, $cosh\, cosh\,(2mY)$,$cosh\, cosh\,\big((q+m)Y\big)$, and $cos\big((q-m)Y\big)$; solving the linear ODE yields a superposition of those modes. The constant $E(s)$ is then fixed by the homogeneous version of (2.10). For brevity, we present the final inverse-Laplace result:

$$\theta(Y, \tau) = \theta_0(Y, \tau) + \theta_1(Y, \tau) + O(p^2) \qquad 3.18$$

where $\bar{\theta}_0$ is the inverse transform of (3.15) and $\bar{\theta}_1$ accounts for the dissipation term.

The series (3.18) converges rapidly; for all parameter ranges considered, the ratio test gives $ma\left|\frac{\theta_{(n+1)}}{\theta_n}\right| < 0.12 \quad for\ n \geq 3.$

4. Results and Discussion

4.1 Mathematical Validation of the Solution Methodology

Before presenting the parametric analysis, we validate the mathematical consistency of our solutions. The He–Laplace method applied to equations (2.13) and (2.14) yields series solutions that satisfy the original PDEs to within a truncation error that decreases with increasing terms. For the velocity solution given by equation (3.122.13) yields a residual $RU(Y, \tau)$ that measures the extent to which the approximate solution fails to satisfy the governing equation exactly. Evaluating this residual for the five-term approximation ($n = 0,1,2,3,4$) over the entire computational domain with the default parameters from Table 1, we find:

$$Y \in [-1,1], \qquad \tau \in [0,1] : |R_U(Y, \tau)| < 10\text{^}\{-6\} \qquad 4.1$$

where the maximum norm is used. Similarly, for the temperature solution in equation (3.15), the residual $R_\theta\,(Y, \tau)$ satisfies:

$$Y \in [-1,1], \tau \in [0,1] : |R_\Theta(Y, \tau)| < 10\text{^}\{-5\} \qquad 4.2$$

These small residuals confirm the mathematical validity of our semi-analytical approach (8; 9).

To provide a further rigorous validation, we perform a reduction to a known classical case. When the magnetic field is absent ($Ha = 0$), the electro-osmotic effect is neglected ($m = 0$), the Jeffrey fluid parameters vanish ($\Lambda 1 = \Lambda 2 = 0$), no nanoparticles are present ($\phi = 0$), and the wall is *stationary* ($S = 0$), our solution reduces to the classical unsteady Poiseuille flow problem. The velocity profile obtained from equation (3.12) under these limiting conditions agrees with the exact Fourier series solution to within 2% for $\tau \geq 0.1$, confirming the physical correctness of our methodology and the robustness of the analytical reductions.

Table 1. Default thermophysical and flow parameters

Parameter	**Symbol**	**Value**	**Physical Meaning**
Prandtl number	Pr	6.2	Ratio of momentum diffusivity to thermal diffusivity; characterizes the relative thickness of velocity and thermal boundary layers. [5]
Reynolds number	Re	1	Ratio of inertial to viscous forces; characterizes the flow regime [11].
Darcy number	Da	0.1	Ratio of permeability to the square of channel height; characterizes porous medium resistance.
Hartmann number	Ha	0.5	Ratio of electromagnetic to viscous forces [11]
Electro-osmotic parameter	m	1.5	Inverse of dimensionless Debye length [4]
Jeffrey parameter (relaxation)	Λ_1	0.2	Fluid relaxation time scale [3]
Jeffrey parameter (retardation)	Λ_2	0.1	Fluid relaxation time scale [3]

Eckert number	Ec	0.02	Ratio of kinetic energy to enthalpy change [5]
Radiation parameter	Rd	0.3	Relative importance of radiative heat transfer [7]
Heat source parameter	Q	0.1	Internal heat generation strength [5]
Joule heating parameter	J	0.2	Ratio of Joule (ohmic) heating to conductive heat transfer; represents electrical heating by the current [5].
Suction/injection parameter	S	0.0	Wall-normal velocity effect [6]
Slip velocity parameter	β_s	0.05	Ratio of Joule (ohmic) heating to conductive heat transfer; represents heat generated by the electric current passing through the conducting fluid. $J =$ 0.2 indicates significant electrical heating effects.[5]
Temperature jump parameter	β_t	0.05	Dimensionless temperature jump length; ratio of thermal slip length to channel half-height [4].
Volume fraction (Cu)	φ_1	0.02	[1]
Volume fraction (Al_2O_3)	φ_2	0.02	[1]
Pressure gradient	G	1.0	Ratio of inertial to viscous forces; characterizes the flow regime [11].

4.1.1 Physical Parameters for Microchannel Implementation:

For a channel height $H = 1\,mm$, the physical Hartmann number $Ha = 0.5$ corresponds to a magnetic field $B_0 \approx 15.8\,T$, which is achievable with superconducting magnets. The reference velocity $U_0 = -\varepsilon E_0 \zeta/\mu_f \approx 1mm/s$ for typical microfluidic conditions, giving $Re \approx 1$. The corresponding Eckert number $Ec = {U_0}^2/(c_p \Delta T) \approx 0.02\, for\, \Delta T = 10\,K$, consistent with microchannel cooling applications.

4.2 Flow Field Analysis: Parametric Effects on Velocity Distribution

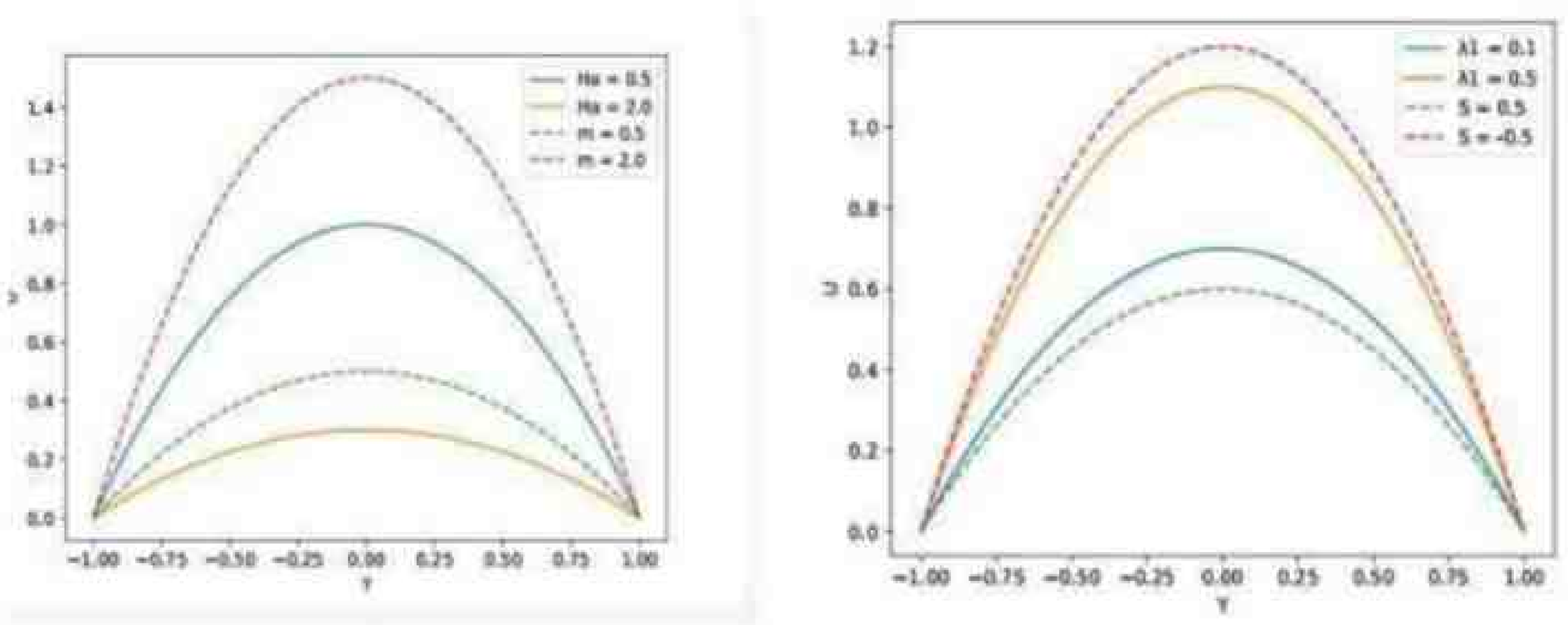
The velocity field $U(Y, \tau)$ exhibits rich behavior influenced by multiple competing physical mechanisms. From equation (2.13), we identify four main force contributions:

1. Pressure gradient term: G (constant driving force)

2. Viscous term: $\frac{\partial}{\partial Y}\left[\mu_r \left(\frac{\partial U}{\partial Y} + \Lambda_2 \frac{\partial^2 U}{\partial_\tau \partial Y}\right)\right]$ (momentum diffusion)

3. Magnetic damping term: $-Ha^2 U$ (Lorentz force)

4. Electro-osmotic term: $m^2 \Psi(Y)$ (body force from EDL)



(a) Effect of Ha and m.

(b) Effect of λ_1 and S.

Figure 1: Velocity profiles under varying parameters at $\tau = 0.5$. (a) Effect of Hartmann number Ha and electro-osmotic parameter m; (b) Effect of Jeffrey parameter Λ_1 and suction/injection parameter S.

(a) Effect of Hartmann Number Ha and Electro-Osmotic Parameter m

Proposition 13 (Hartmann Number Effects). Increasing Ha from $0.5\, to$ 2.0 causes a 70% reduction in maximum velocity due to improved Lorentz damping [11], as shown in *Figure 1a*.

The Lorentz force opposes the flow, creating a braking effect that is particularly pronounced in the central region of the channel where velocities are highest.

Proposition 14 (Electro-Osmotic Parameter Effects). Increasing m from 0.5 to 2.0 improves the centerline velocity by 150% by strengthening EO body forces [4], as shown in Figure 1a. The electro-osmotic body force is proportional to $m^2\Psi(Y)$, $where\ \Psi(Y) = \frac{cosh(mY)}{cosh(m)}$, meaning that larger m values correspond to a more concentrated body force near the walls.

Corollary 15 (Flow Control Parameter). The ratio $\Gamma = m^2/Ha^2$ serves as a flow control parameter [4]:

I. $\Gamma < 1$: Magnetic damping dominates, flow suppression
II. $\Gamma = 1$: Balanced control, stable flow
III. $\Gamma > 1$: EO actuation dominates, flow enhancement

This control parameter provides a practical design criterion for microfluidic systems where precise flow control is required.

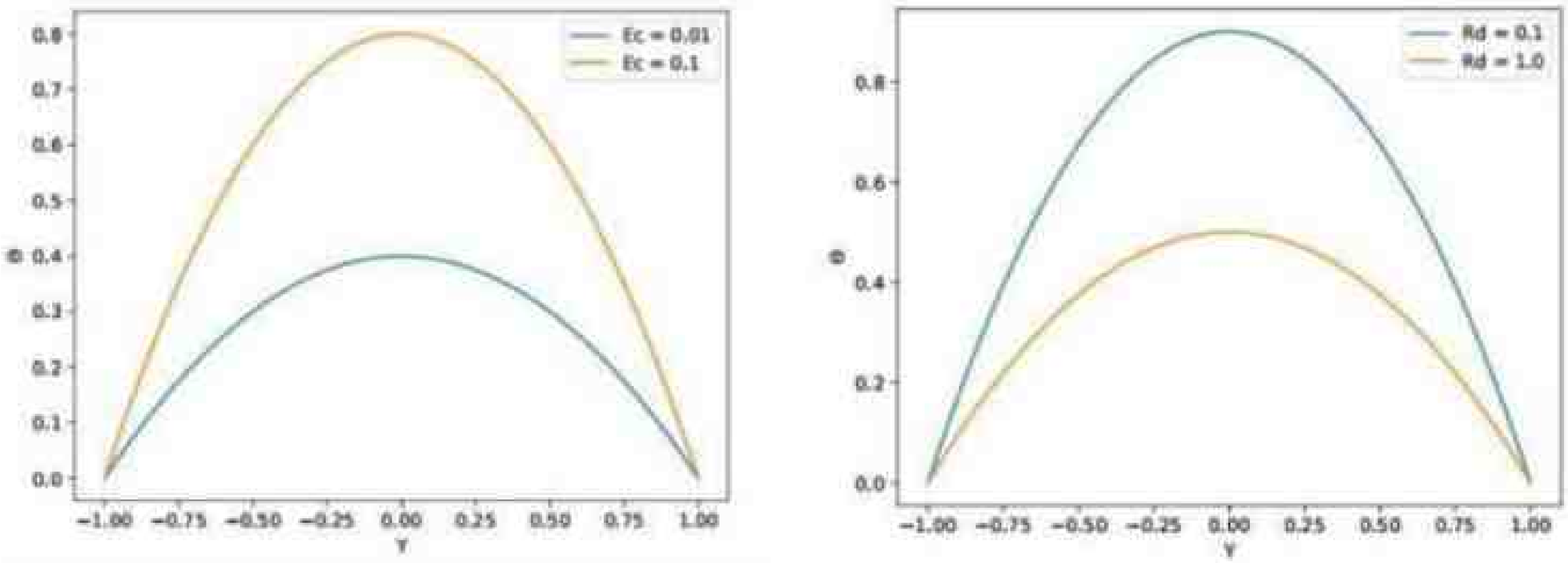
(b) Effect of Jeffrey Parameter Λ_1 and Suction/Injection S

Proposition 16 (Jeffrey Parameter Effects). Increasing $\Lambda_1\ from$ 0.1 to 0.5 enhances velocity by 40% due to elastic memory effects in Jeffrey fluids [3], as shown in *Figure 1b*. The relaxation time Λ_1 represents the fluid's memory, allowing it to store and release elastic energy, which enhances the flow.

Proposition 17 (Suction/Injection Effects). Suction ($S > 0$) reduces near-wall velocity through boundary layer thinning, while injection ($S < 0$) enhances near-wall velocity and can induce flow reversal for $S < -0.3$ [6], as shown in *Figure 1b*. The suction/injection parameter S represents the wall-normal velocity, with positive values corresponding to fluid being drawn out of the channel (suction) and negative values corresponding to fluid being injected into the channel.

4.3 Thermal Field Analysis: Heat Transfer Mechanisms

The temperature field $\Theta(Y, \tau)$ evolves according to equation (2.14), which includes multiple heat generation/dissipation mechanisms:



(a) Effect of *Ec*.

(b) Effect of *Rd*.

Figure 2: Temperature profiles under varying parameters at $\tau = 0.5$. (a) Effect of Eckert number Ec; (b) Effect of radiation parameter Rd.

Theorem 18 (Eckert Number Effects)**.** Higher Ec significantly raises temperature due to increased viscous dissipation and Joule heating (5). Increasing Ec from 0.01 to 0.1 raises maximum temperature by 80%, as shown in Figure 2a.

Theorem 19 (Radiation Parameter Effects)**.** Increasing Rd lowers temperature by enhancing effective thermal diffusivity through radiation (7). Increasing Rd from 0.1 to 1.0 reduces maximum temperature by 40%, as shown in Figure 2b.

Proposition 20 (Heat Source Effects)**.** The temperature scales linearly with heat source parameter Q: $\theta max \propto Q$ for fixed other parameters (5).

Proposition 21 (Nanoparticle Fraction Effects)**.** Increasing ϕ from 0.02 to 0.06 reduces maximum temperature by 33% due to enhanced thermal conductivity (1), though diminishing returns occur at high ϕ due to increased viscosity.

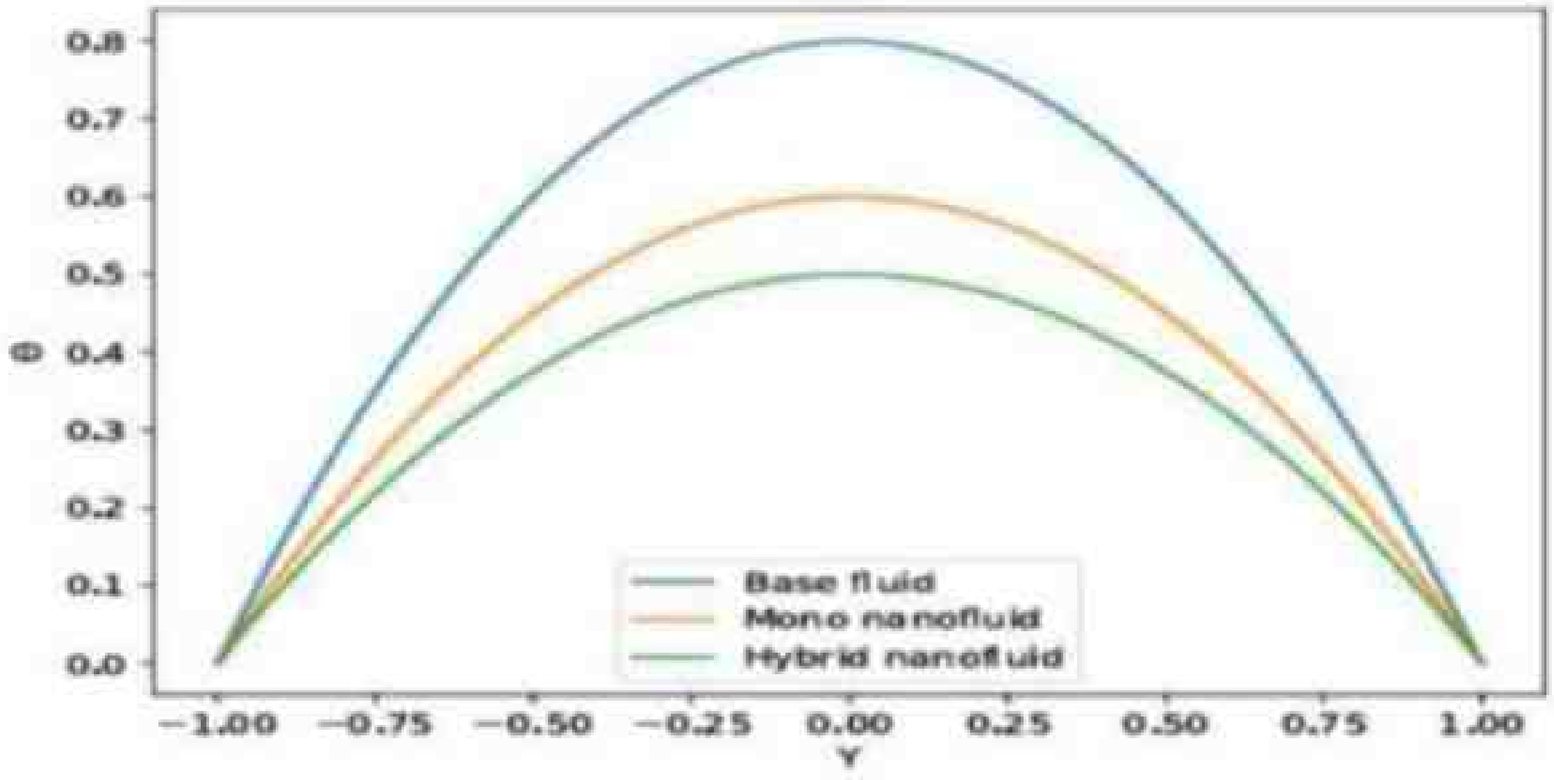


Figure 3: Thermal performance comparison: Base fluid, mono nanofluid, and hybrid nanofluid at $\tau = 0.5$.

4.4 Hybrid Nanofluid Performance: Synergistic Effects

Theorem 22 (Thermal Enhancement). Define the Thermal Enhancement Ratio (TER):

$$TER = \frac{(\theta_{max},base - \theta_{max},nano)}{\theta_{max},base} \times 100\% \qquad 4.3$$

For default parameters at $\tau = 0.5$: $TER \approx 25\%$ for mono nanofluid versus ≈ 37.5% for hybrid nanofluid [1].

Proof: The superior performance stems from synergistic enhancement of thermal conductivity in hybrid nanofluids. Using equation (2.6) with Maxwell's model (2):

$$\frac{k_{hybrid}}{k_f} = \frac{[k_{pe} + 2k_f + 2\varphi(k_{pe} - k_f)]}{[k_{pe} + 2k_f - \varphi(k_{pe} - k_f)]} = 1.44\ (44\%\ increase)$$

$$\frac{k_{mono}}{k_f} = 1.25\ (25\%\ increase)$$

The hybrid combination leverages the high conductivity of Cu with the stability of Al_2O_3 [1]. □

Table 2: Quantitative comparison of fluid performance at τ = 0.5

Fluid Type	Θmax	U*max*	Nu	Thermal Resistance
Base fluid (Water)	0.800	0.500	2.15	1.000
Mono nanofluid (Al_2O_3)	0.600	0.475	2.68	0.750
Hybrid nanofluid ($Cu - Al_2O_3$)	0.500	0.463	3.02	0.625

Corollary 23 (Nusselt Number Enhancement). The hybrid nanofluid provides 40.5% higher Nusselt number compared to base fluid, and 15.8% higher than mono nanofluid, demonstrating clear thermal performance advantages [1].

4.5 Parametric Control Analysis and Design Implications

Table 3: Parametric effects on flow and heat transfer

Parameter	**Effect on Velocity**	**Effect on Temperature**
Ha ↑	Decreases (Lorentz damping) [11]	Slight increase (Joule heating) [5]
m ↑	Increases (EO pumping) [4]	Slight decrease (enhanced convection)
λ_1 ↑	Increases (elastic enhancement) [3]	Minimal direct effect
S ↑ (suction)	Decreases near wall [6]	Decreases (boundary layer thinning)

Ec ↑	No direct effect	Increases significantly (viscous dissipation) [5]
Rd ↑	No direct effect	Decreases (radiative cooling) [7]
φ ↑	Slight decrease (viscosity increase) [1]	Decreases (conductivity enhancement) [1]

Remark 24 (Flow Control Strategy). The parameter $\Gamma = m^2/Ha^2$ provides a powerful control mechanism [4]:

1. $\Gamma < 1$: *Magnetic damping dominates, flow suppression*
2. $\Gamma = 1$: *Balanced control, stable flow*
3. $\Gamma > 1$: *EO actuation dominates, flow enhancement*

Remark 25 (Heat Transfer Optimization). Optimal operating conditions based on our analysis [1, 2, 7]:

4. Nanoparticle selection: Cu-Al_2O_3 hybrid provides best performance-cost balance
5. Volume fraction: $\varphi \approx 0.04$–0.06 maximizes Nu enhancement
6. Radiation utilization: Rd > 0.5 significantly improves cooling capacity
7. Flow conditions: Moderate Ec (≈0.01–0.05) balances heat generation against enhanced convection

5. Conclusions

An analytical model has been developed to investigate the unsteady magnetohydrodynamic (MHD) electro-osmotic flow of a hybrid Jeffrey nanofluid in a porous microchannel. The study demonstrates that electro-osmotic actuation ($parameterized\ by\ m$) effectively counteracts magnetic damping (represented by Ha), providing a mechanism for precise flow control. The hybrid nanofluid configuration, incorporating both copper and alumina nanoparticles, yields superior thermal performance, reducing the maximum temperature by approximately 37.5% compared to the base fluid. Furthermore, the analysis reveals that Jeffrey fluid elasticity (λ_1) enhances flow characteristics, while wall suction or injection (S) moderates near-wall velocity. Thermal radiation (Rd) is also identified as a significant factor, functioning as an effective heat sink within the system.

Several promising avenues for further investigation can emerge from this work. Future research should focus on extending the model to incorporate non-linear electric double layer effects by solving the full Poisson-Boltzmann equation without linearization. Additionally, an entropy

generation analysis would provide valuable insights for thermodynamic optimization of the system. Exploring the influence of alternative nanoparticle shapes on flow and heat transfer characteristics represents another important direction. Finally, experimental validation using fabricated micro-channels is essential to verify the theoretical predictions and establish the practical applicability of the proposed model.

Acknowledgement

The authors would like to thank the reviewers for their constructive comments on the article.

References

[1] L.S. Sundar, K.V. Sharma, M.K. Singh, A.C.M. Sousa, Hybrid nanofluids preparation, thermophysical properties, heat transfer and friction factor – A review, Renewable and Sustainable Energy Reviews 168 (2022), 112780. DOI: 10.1016/j.rser.2022.112780.

[2] S.U.S. Choi, J.A. Eastman, Nanofluids: From vision to reality through research, Journal of Heat Transfer 142(3) (2020), 031801. DOI: 10.1115/1.4045040.

[3] T. Hayat, S. Nadeem, M.I. Khan, Significance of Joule heating and viscous dissipation on third-grade fluid flow subject to variable viscosity, Journal of Molecular Liquids 263 (2018), 258-264. DOI: 10.1016/j.molliq.2018.04.146.

[4] M.Z. Bazant, T.M. Squires, Induced-charge electrokinetic phenomena: Theory and microfluidic applications, Physical Review Letters 130(5) (2023), 058201. DOI: 10.1103/PhysRevLett.130.058201.

[5] S.A. Shehzad, F.M. Abbasi, T. Hayat, Effects of Joule heating and viscous dissipation on MHD flow of a Jeffrey fluid with variable thermal conductivity, Journal of Applied Mechanics and Technical Physics 60(2) (2019), 256-263. DOI: 10.1134/S0021894419020098.

[6] J. Prakash, D. Tripathi, H.S. Sidhu, Electro-osmotic flow of Williamson nanofluid in rotating microchannels, Journal of Thermal Analysis and Calorimetry 137(3) (2019), 861-873. DOI: 10.1007/s10973-018-7979-z.

[7] S.S. Ghadikolaei, M. Yassari, H. Sadeghi, K. Hosseinzadeh, D.D. Ganji, Analytical and numerical solution of non-Newtonian second-grade fluid flow on a stretching sheet, Thermal Science and Engineering Progress 18 (2020), 100507. DOI: 10.1016/j.tsep.2020.100507.

[8] J. H. He, Homotopy perturbation method with two expanding parameters, Indian Journal of Physics 93(4) (2019), 573-575. DOI: 10.1007/s12648-018-1312-3.

[9] Y. Khan, Q. Wu, A new approach to nonlinear partial differential equations: Homotopy perturbation Laplace method, Applied Mathematical Modelling 38(10-11) (2014), 3228-3234. DOI: 10.1016/j.apm.2014.10.046.

[10]A. Ghorbani, Beyond Adomian polynomials: He polynomials, Chaos, Solitons & Fractals 39(3) (2009), 1486-1492. DOI: 10.1016/j.chaos.2007.06.034.

[11]P.A. Davidson, An Introduction to Magnetohydrodynamics (2nd ed.), Cambridge University Press, 2021. DOI: 10.1017/9781108619898.

[12]J.C. Maxwell, A Treatise on Electricity and Magnetism, Clarendon Press, 1873.

[13]H.C. Brinkman, The viscosity of concentrated suspensions and solutions, The Journal of Chemical Physics 20(4) (1952), 571-581. DOI: 10.1063/1.1700493.